

Non-invasive imaging of object behind turbid media via cross-spectrum

Xingchen Zhao,¹ Tao Peng,¹ Zhenhuan Yi,¹ Lida Zhang,^{1,2} M. Suhail Zubairy,¹ Yanhua Shih,³ and Marlan O. Scully^{1,4,5}

¹*Department of Physics and Astronomy, Texas A&M University, College Station, TX 77843, USA*

²*Department of Physics and Astronomy, Aarhus University, 8000 Aarhus C, Denmark*

³*Department of Physics, University of Maryland, Baltimore County, Baltimore, Maryland 21250, USA*

⁴*Baylor Research and Innovation Collaborative, Baylor University, Waco, TX 76706, USA*

⁵*Princeton University, Princeton, NJ 08544, USA*

(Dated: 29 May 2022)

We develop a method based on the cross-spectrum of an intensity-modulated CW laser, which can extract a signal from an extremely noisy environment and image objects hidden in turbid media. We theoretically analyzed our scheme and performed the experiment by scanning the object placed in between two ground glass diffusers. The image of the object is retrieved by collecting the amplitudes at the modulation frequency of all the cross-spectra. Our method is non-invasive, easy-to-implement, and can work for both static and dynamic media.

Optical observation through inhomogeneous media is a difficult task in optics^{1–3}. Imaging through highly disordered media is especially challenging. Multiple scattering introduced by these media, such as turbid fluids and biological tissues, can attenuate light intensity dramatically and randomize the direction of propagation^{4,5}. A variety of strategies have been devised to image objects hidden behind highly disordered media with different scattering properties. Some methods attempt to extract the non-scattered photons, such as time-gating^{6–9}, coherence-gating^{10–12}, and rotating polarization methods^{13–15}. These techniques suffer from low signal-to-noise ratio due to the tiny amount of non-scattered photons, which greatly limits the imaging (or penetration) depth. In addition, some gating techniques require the use of ultrafast laser pulses, which may be devastating for living biological tissue. Other methods focus on reversing the scattering process and recover input optical information directly from scattered photons, such as optical phase conjugation^{16,17}, transmission matrix^{18–20}, and speckle correlation^{21–23}. However, these methods are either invasive or require intensive computations using iterative algorithms that can only work for static media. Imaging through dynamic media is still quite challenging^{23–26}. In this case, the time-dependent mapping between input and output fields requires instant completion of the image reconstruction process to follow the variation of media. Therefore, the capability of iterative algorithms is greatly reduced.

In this letter, we report a novel method based on the cross-spectrum measurement of an intensity-modulated CW laser. The cross-spectrum technique has been mainly used to analyze the cross-correlation between two time series in the frequency domain. We adopt this technique to demonstrate a non-invasive and easy-to-implement scheme, by which the image of an object can be reconstructed not only through both static and dynamic diffusers but also under extremely noisy environment, *i.e.*, the light intensity is much lower than detector noise. Besides, the use of CW laser makes the method more favorable in applications involving living tissues.

The experimental setup is shown in Fig. 1. A CW laser

is intensity-modulated by an electro-optic modulator (EOM) at frequency $f_0 = 1$ MHz. An objective lens (L1) is used to focus the modulated light onto the object plate ‘1X’ that is sandwiched in situ between a pair of ground glass diffusers (GGDs) of 220 grit (average grit diameter $\bar{d}_{\text{grit}} = 53$ μm , thickness of 2 mm each). A second lens (L2) is placed behind GDD2 to collect the scattered light. The distance between the object and each diffuser is ~ 5 mm. The GGDs can be either kept static or moved back and forth by a motorized stage. The output light is split into two arms by a beam splitter (BS), which are then measured by two photodetectors (PDs) respectively, where the two PDs (Thorlabs, PDA 10A) are put at the focal plane of the lens. The data is then sent to a computer to generate images of the object. The object is scanned pixel-by-pixel with an appropriate step size to resolve the region of interest. We note here that, due to the low incident laser power (~ 2 μW) and strong scattering from the two GGDs (~ 75 nW at the detector plane), the laser power measured at each PD is buried in the electronic and environmental noise.

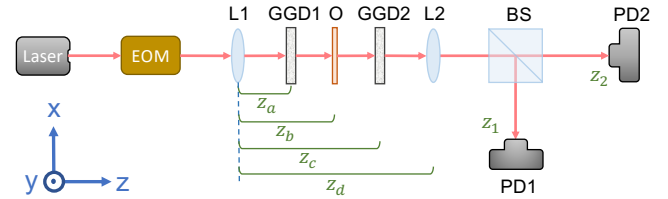


FIG. 1. Schematic of the experimental setup. We use a modulated CW laser for illumination. The object is sandwiched between two GGDs. Signal at each detector is made to be much lower than the noise level. EOM: electro-optic modulator; L: lens; GGD: ground glass diffuser; O: object; BS: beam splitter; PD: photodetector. The Cartesian coordinate is located in the center of L1 with z -axis pointing along the propagation direction of the light. z_1 and z_2 are the distances between L1 and the two PDs, respectively.

We first outline a theoretical description of the cross-spectrum method^{27–30}. As shown in Fig. 1, a Cartesian coordinate system is placed in the center of L1, with the z -axis

pointing along the propagation direction of the light. A collimated incident beam of radius σ is focused by L1 with focal length f_1 . The scattering centers on GGD1 will produce an electric field at distance z with the form

$$E(\rho_z, z, t) = \frac{-ik}{2\pi} A(z - z_a) \times \int d^2 \rho_{z_a} E(\rho_{z_a}, z_a, t) R(\rho_{z_a}) G(\rho_z - \rho_{z_a}; z - z_a), \quad (1)$$

where $\rho_{z_a} = (x_{z_a}, y_{z_a})$ is a position vector in the in GGD1 plane, k is the wave vector, $R(\rho_{z_a})$ describes GGD1 as a phase plate due to the scattering centers at ρ_{z_a} , which imprint the random phase profile on the propagating field. We also define $A(z) = e^{ikz}/z$, $G(\alpha; \beta) = e^{ik\alpha^2/2\beta}$, and

$$E(\rho_{z_a}, z_a, t) = E_0(t) E_a e^{-i(v_0 t - k z_a)} \times \exp \left\{ -\frac{E_a}{2} \left(\frac{ik}{f_1} + \frac{1}{2\sigma^2} \right) \rho_{z_a}^2 \right\}, \quad (2)$$

in which $E_0(t) = \sqrt{I_0} \cos 2\pi f_{mod} t$ expresses a sinusoidal modulation of light intensity I_0 at frequency f_{mod} , and $E_a = -\frac{ik}{2z_a} \frac{1}{1/4\sigma^2 + (ik/2)(1/f - 1/z_a)}$. v_0 is the frequency of the laser. $\rho_z = (x_z, y_z)$ is the position vector in the receiver plane at distance z from L1. The integration in Eq. (1) is performed over the illumination area on GGD1.

Since the object is scanned point by point and the light path is fixed during the scan, we can model the object as a transmission function $T(\rho_{z_b})$ where $\rho_{z_b} = (x_{z_b}, y_{z_b})$ is the position vector in the object plane. Upon passing through the object, being scattered by GGD2, and being collected by L2, the field at the two detectors is found to be

$$E(z_j, t) = \frac{-ik}{2\pi} \tilde{A} \iiint d^2 \rho_{z_j} d^2 \rho_{z_d} d^2 \rho_{z_c} d^2 \rho_{z_a} \times E(\rho_{z_a}, z_a, t) R(\rho_{z_a}) R(\rho_{z_c}) T(\rho_{z_b}) \times G(\rho_{z_c} - \rho_{z_a}, z_c - z_a) G(\rho_{z_d} - \rho_{z_c}, z_d - z_c) \times G(\rho_{z_j} - \rho_{z_d}, z_j - z_d) G(-\rho_{z_d}, f_2), \quad (3)$$

where $\tilde{A} = A(z_c - z_a) A(z_d - z_c) A(z_j - z_d)$, z_j ($j = 1, 2$) denote the distance between the detector j and L1, f_2 is the focal length of L2, $R(\rho_{z_c})$ describes the random phase profile due to scattering on GGD2. $G(-\rho_{z_d}; f_2)$ is the propagation factor of L2.

The total signals measured by the two photodetectors can be expressed as

$$S(z_j, t) = I(z_j, t) + \beta_j N(t), \quad (4)$$

where $I(z_j, t) \equiv E(z_j, t) E^*(z_j, t)$ is the intensity at detector j , $N(t)$ is a white noise distribution that models all the noise due to detectors and environment, and β_j is the amplitude of the noise at detector j . It follows that the time-domain cross-correlation is given by

$$C(\tau) = \left\langle \int_0^{\mathcal{T}} dt S^*(z_1, t) S(z_2, t + \tau) \right\rangle, \quad (5)$$

where \mathcal{T} is the measurement time. We further assumed that the correlations between intensity and noise vanish since they are uncorrelated. On substituting from Eq. (4) into Eq. (5), we obtain

$$C(\tau) = \int_0^{\mathcal{T}} dt \langle I(z_1, t) I(z_2, t + \tau) \rangle + \beta_1 \beta_2 \int_0^{\mathcal{T}} dt \langle N(t) N(t + \tau) \rangle. \quad (6)$$

The intensity correlation in the first term of Eq. (6) can be expressed as

$$\langle I(z_1, t) I(z_2, t + \tau) \rangle = \langle E(z_1, t) E^*(z_1, t) E(z_2, t + \tau) E^*(z_2, t + \tau) \rangle \quad (7)$$

where $E(z_j, t)$ ($j = 1, 2$) is given by Eq. (3). Since the scattering centers are independent of each other and satisfy Gaussian statistics, the random phase term $R(\rho_{z_i})$ obeys

$$\langle R(\rho_{z_i}) R^*(\rho'_{z_i}) \rangle = \delta(\rho_{z_i} - \rho'_{z_i}) \quad (8)$$

and

$$\langle R(\rho_{z_i}) R^*(\rho'_{z_i}) R(\rho''_{z_i}) R^*(\rho'''_{z_i}) \rangle = \delta(\rho_{z_i} - \rho'_{z_i}) \delta(\rho''_{z_i} - \rho'''_{z_i}) + \delta(\rho_{z_i} - \rho'''_{z_i}) \delta(\rho'_{z_i} - \rho''_{z_i}) \quad (9)$$

where $i = a, c$ and $\delta(\rho - \rho')$ is the delta function. The second term in Eq. (6) is given by³¹

$$\int_0^{\mathcal{T}} dt \langle N(t) N(t + \tau) \rangle = \delta(\tau). \quad (10)$$

Upon substituting Eq. (2), (3), and (7) – (10) into Eq. (6), we obtain after carrying out the integrations

$$C(\tau) \propto \mathcal{T} |T(\rho_{z_b})|^4 \cos(2\pi f_{mod} \tau) + \beta_1 \beta_2 \delta(\tau). \quad (11)$$

It follows from Eq. (11) that the cross-correlation is

$$\Gamma(\rho_{z_b}; \omega) = \int_{-\infty}^{\infty} C(\tau) e^{-i\omega \tau} d\tau = \Gamma_0 \mathcal{T} |T(\rho_{z_b})|^4 \delta(\omega - 2\pi f_{mod}) + \beta_1 \beta_2, \quad (12)$$

where

$$\Gamma_0 = \left(\frac{4\pi^2}{k^2} \right)^2 \frac{(\pi\sigma^2)^2 |\tilde{A}|^4 I_0^2}{f_{mod}}. \quad (13)$$

The cross-spectrum is a sum of frequency peak signal multiplied by $|T(\rho_{z_b})|^2$ and uniform noise background. Note the pattern on the object can be represented by $|T(\rho_{z_b})|^2$. Scanning the object and recording $S_1(t)$ and $S_2(t)$ at every position ρ_{z_b} , we can calculate the cross-spectrum as a function of position and get an image of the pattern by plotting $\Gamma(\rho_{z_b}; \omega = 2\pi f_{mod})$. The reason why this scheme works is simple: at every position where the pattern does not exist, the light will be blocked ($|T(\rho_{z_b})|^2 \equiv 0$) and hence no modulation frequency can be detected; while, at every position where

the pattern exists ($|T(\rho_{zb})|^2 \equiv 1$), light can go through and the modulation frequency can be found by Eq. (12). Furthermore, the larger the integration time \mathcal{T} is, the greater the amplitude of the frequency peak will be; while, the noise is independent of \mathcal{T} . This suggests that, by increasing \mathcal{T} , the signal-to-noise ratio can be enhanced. Therefore, even though the output signal may undergo multiple scattering by the media and is below the noise level of the detectors, this method can still reconstruct the image of the target.

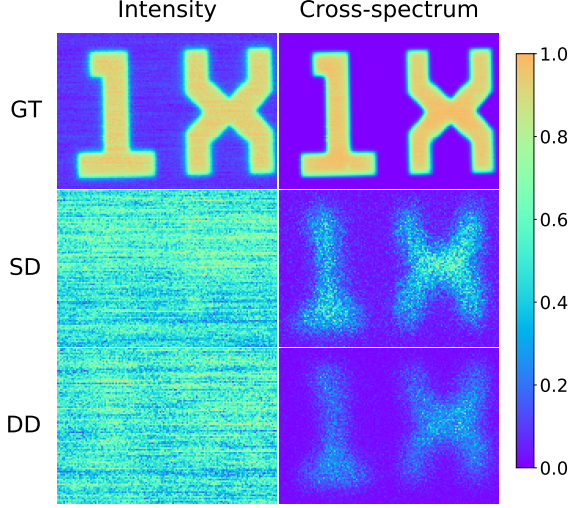


FIG. 2. Raster-scan images for an object of millimeter size with the letter "IX" being transparent and other regions being opaque. Cross-spectrum images are generated by plotting $\Gamma(\rho_{zb}; \omega = 2\pi f_{mod})$ (see Eq. (12)). GT: ground truth. SD: static diffuser. DD: dynamic diffuser.

TABLE I. Visibility for different diffuser states

Diffuser State	Intensity	Cross-spectrum
Ground truth (GT)	0.725	0.967
Static diffuser (SD)	0.032	0.451
Dynamic diffuser (DD)	0.031	0.558

To demonstrate that our method works experimentally for both static and dynamic turbid media, we perform the measurements under three situations: 1. imaging without diffuser (ground truth, GT); 2. the object is sandwiched between two static diffusers (SDs); and 3. the two diffusers are moved back and forth by a motorized stage (dynamic diffusers, DDs). The object has the letter "IX" being transparent and other regions being opaque. For all three cases, data are collected by an oscilloscope with a fixed sample rate at 2 GHz. At each position, 1 million data points are taken to calculate the cross-spectrum, corresponding to 500 μs integration time which ensures a strong cross-correlation signal. The whole image contains 100 by 140 pixels with the pixel size of 25 μm .

The main experimental result is shown in Fig. 2, of which the pixel values v are normalized by $\tilde{v} = (v - v_{min}) / (v_{max} - v_{min})$. In the first column, we directly plot the intensity mea-

sured by the detectors; while, in the second column, we plot $\Gamma(\rho_{zb}; 2\pi f_{mod})$. The first row shows GT images. The second and third row list images obtained with SD and DD, respectively. We summarize the visibility of images in Table I, which is calculated by $V = (\bar{v}_s - \bar{v}_b) / (\bar{v}_s + \bar{v}_b)$, where \bar{v}_s and \bar{v}_b are the average pixel values of signal ("IX" region) and background, respectively. As shown in Fig. 2, in both SD and DD cases, when the strong scattering media is present, the recorded intensity does not show any image in either case, the extremely low visibility is a sign that our signal is truly at the noise level of the detectors. On the other hand, in both cases, the images are still retrieved using the cross-spectrum technique with high visibility. The results suggest that the cross-spectrum method can image an object hidden behind both static and dynamic strong scattering media. We also notice that the visibility of the cross-spectrum image is higher than the intensity image even though there is no diffuser (GT), which suggests cross-spectrum is also an effective way to enhance signal-to-noise ratio when the scattering media is absent.

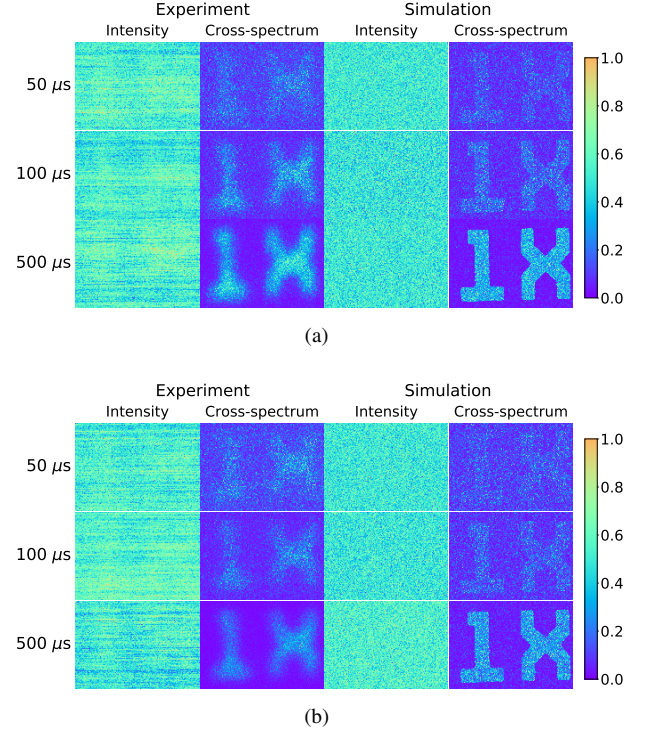


FIG. 3. Raster-scan images and simulations for different acquisition time with (a) static diffusers and (b) dynamic diffusers.

To further exam our method, we also compare the measured images from different acquisition time (50 μs , 100 μs , and 500 μs) with the same sample rate. The incident intensity of light is fixed for the static and rotating diffusers. Simulation is also performed for the intensity and cross-spectrum based on Eq. (4) and Eq. (12), respectively, as a comparison with the experimental results. The results are shown in Fig. 3, the corresponding visibility of the experimental results are listed in Table II. It can be seen that, in general, the longer integration

TABLE II. Visibility of different acquisition time for static and dynamic diffuser states

Acquisition time	Static diffuser (SD)		Dynamic diffuser (DD)	
	Intensity	Cross-spectrum	Intensity	Cross-spectrum
50 μ s	0.027 ± 0.004	0.135 ± 0.009	0.035 ± 0.005	0.190 ± 0.004
100 μ s	0.033 ± 0.004	0.332 ± 0.001	0.030 ± 0.002	0.305 ± 0.004
500 μ s	0.034 ± 0.003	0.466 ± 0.008	0.048 ± 0.004	0.560 ± 0.002

time is, the higher visibility one can achieve for both static and rotating diffusers. This means we can obtain a clear image under strong scattering at the expense of long acquisition time. We note that the visibility of the recorded intensity image is kept extremely low even when one increases the acquisition time up to 10 times, nevertheless the cross-spectrum image becomes more and more clear. The visibility also increases much faster than that of the intensity measurement when increasing the acquisition time. We point out that the fundamental limit of imaging speed is the acquisition length, which is on the order of 100 μ s for the current setup, but can be in principle orders faster with higher modulation frequency and higher sample rate (GHz range laser modulation speed and detection). The raster scan speed can also be much improved if, for instance, a 2D galvo-resonant scanner is integrated into the system.

In conclusion, we have developed a cross-spectrum method to extract a weak optical signal from the extremely noisy background and image objects hidden behind scattering media. The major advantage of this scheme is that it uses CW laser with low power in a non-invasive manner which would be easy to implement and bio-tissue friendly. It suits for both static and dynamic media, which makes it adaptive in most application situations. Together with the fast acquisition time with current technology, our scheme paves the way for efficient imaging in previously inaccessible scenarios.

ACKNOWLEDGEMENTS

This research is supported by grants from: Air Force Office of Scientific Research (Award No. FA9550-20-1-0366 DEF), Office of Naval Research (Award No. N00014-20-1-2184), Robert A. Welch Foundation (Grant No. A-1261), National Science Foundation (Grant No. PHY-2013771), King Abdulaziz City for Science and Technology (KACST). The authors thank Y. J. Shen and T. Smith for helpful discussions.

DATA AVAILABILITY

The data that support the findings of this study are available upon reasonable request.

¹R. E. Meyers, K. S. Deacon, and Y. Shih, "Turbulence-free ghost imaging," *Appl. Phys. Lett.* **98**, 111115 (2011).

²A. P. Mosk, A. Lagendijk, G. Lerosey, and M. Fink, "Controlling waves in space and time for imaging and focusing in complex media," *Nature Photonics* **6**, 283–292 (2012).

³S. Rotter and S. Gigan, "Light fields in complex media: Mesoscopic scattering meets wave control," *Rev. Mod. Phys.* **89**, 015005 (2017).

⁴V. Gopal, S. Mujumdar, H. Ramachandran, and A. K. Sood, "Imaging in turbid media using quasi-ballistic photons," *Optics Communications* **170**, 331–345 (1999).

⁵V. Ntziachristos, "Going deeper than microscopy: The optical imaging frontier in biology," *Nature Methods* **7**, 603–614 (2010).

⁶L. Wang, P. P. Ho, C. Liu, G. Zhang, and R. R. Alfano, "Ballistic 2-D Imaging Through Scattering Walls Using an Ultrafast Optical Kerr Gate," *Science* **253**, 769–771 (1991).

⁷M. R. Hee, J. A. Izatt, J. M. Jacobson, J. G. Fujimoto, and E. A. Swanson, "Femtosecond transillumination optical coherence tomography," *Opt. Lett.*, **OL 18**, 950–952 (1993).

⁸B. B. Das, K. M. Yoo, and R. R. Alfano, "Ultrafast time-gated imaging in thick tissues: A step toward optical mammography," *Opt. Lett.*, **OL 18**, 1092–1094 (1993).

⁹F. Liu, K. M. Yoo, and R. R. Alfano, "Transmitted photon intensity through biological tissues within various time windows," *Opt. Lett.*, **OL 19**, 740–742 (1994).

¹⁰N. H. Abramson and K. G. Spears, "Single pulse light-in-flight recording by holography," *Appl. Opt.*, **AO 28**, 1834–1841 (1989).

¹¹H. Chen, Y. Chen, D. Dilworth, E. Leith, J. Lopez, and J. Valdmantis, "Two-dimensional imaging through diffusing media using 150-fs gated electronic holography techniques," *Opt. Lett.*, **OL 16**, 487–489 (1991).

¹²E. Leith, H. Chen, Y. Chen, D. Dilworth, J. Lopez, R. Masri, J. Rudd, and J. Valdmantis, "Electronic holography and speckle methods for imaging through tissue using femtosecond gated pulses," *Appl. Opt.*, **AO 30**, 4204–4210 (1991).

¹³H. Ramachandran and A. Narayanan, "Two-dimensional imaging through turbid media using a continuous wave light source," *Optics Communications* **154**, 255–260 (1998).

¹⁴O. Emile, F. Bretenaker, and A. L. Floch, "Rotating polarization imaging in turbid media," *Opt. Lett.*, **OL 21**, 1706–1708 (1996).

¹⁵S. Sudarsanam, J. Mathew, S. Panigrahi, J. Fade, M. Alouini, and H. Ramachandran, "Real-time imaging through strongly scattering media: Seeing through turbid media, instantly," *Scientific Reports* **6**, 25033 (2016).

¹⁶M. Cui and C. Yang, "Implementation of a digital optical phase conjugation system and its application to study the robustness of turbidity suppression by phase conjugation," *Opt. Express*, **OE 18**, 3444–3455 (2010).

¹⁷Z. Yaqoob, D. Psaltis, M. S. Feld, and C. Yang, "Optical phase conjugation for turbidity suppression in biological samples," *Nature Photonics* **2**, 110–115 (2008).

¹⁸S. M. Popoff, G. Lerosey, R. Carminati, M. Fink, A. C. Boccara, and S. Gigan, "Measuring the Transmission Matrix in Optics: An Approach to the Study and Control of Light Propagation in Disordered Media," *Phys. Rev. Lett.* **104**, 100601 (2010).

¹⁹J. Yoon, K. Lee, J. Park, and Y. Park, "Measuring optical transmission matrices by wavefront shaping," *Opt. Express*, **OE 23**, 10158–10167 (2015).

²⁰M. Kim, W. Choi, Y. Choi, C. Yoon, and W. Choi, "Transmission matrix of a scattering medium and its applications in biophotonics," *Opt. Express*, **OE 23**, 12648–12668 (2015).

²¹J. A. Newman, Q. Luo, and K. J. Webb, "Imaging Hidden Objects with Spatial Speckle Intensity Correlations over Object Position," *Phys. Rev. Lett.* **116**, 073902 (2016).

²²J. Bertolotti, E. G. van Putten, C. Blum, A. Lagendijk, W. L. Vos, and A. P. Mosk, "Non-invasive imaging through opaque scattering layers," *Nature* **491**, 232 (2012).

- ²³O. Katz, P. Heidmann, M. Fink, and S. Gigan, “Non-invasive single-shot imaging through scattering layers and around corners via speckle correlations,” *Nat Photon* **8**, 784–790 (2014).
- ²⁴Y. Yuan and H. Chen, “Non-invasive dynamic or wide-field imaging through opaque layers and around corners,” arXiv:1712.08576 [physics] (2017), arXiv:1712.08576 [physics].
- ²⁵Y. Sun, J. Shi, L. Sun, J. Fan, and G. Zeng, “Image reconstruction through dynamic scattering media based on deep learning,” *Opt. Express*, OE **27**, 16032–16046 (2019).
- ²⁶H. Ruan, Y. Liu, J. Xu, Y. Huang, and C. Yang, “Fluorescence imaging through dynamic scattering media with speckle-encoded ultrasound-modulated light correlation,” *Nature Photonics* , 1–6 (2020).
- ²⁷L. E. Estes, L. M. Narducci, and R. A. Tuft, “Scattering of Light from a Rotating Ground Glass*,” *J. Opt. Soc. Am.*, JOSA **61**, 1301–1306 (1971).
- ²⁸J. H. Churnside, “Speckle from a rotating diffuse object,” *J. Opt. Soc. Am.*, JOSA **72**, 1464–1469 (1982).
- ²⁹J. W. Goodman, *Speckle Phenomena in Optics: Theory and Applications* (Roberts and Company Publishers, 2007).
- ³⁰J. T. Foley and M. S. Zubairy, “The directionality of gaussian Schell-model beams,” *Optics Communications* **26**, 297–300 (1978).
- ³¹J. J. Shynk, *Probability, random variables, and random processes: theory and signal processing applications* (Wiley, 2013).